
CONSTRAINED ATTRACTOR SELECTION USING DEEP REINFORCEMENT LEARNING

A PREPRINT

Xue-She Wang, James D. Turner & Brian P. Mann
 Dynamical Systems Research Laboratory
 Department of Mechanical Engineering & Materials Science
 Duke University
 Durham, NC 27708, USA
 xueshe.wang@duke.edu

July 19, 2022

ABSTRACT

This paper describes an approach for attractor selection in nonlinear dynamical systems with constrained actuation. Attractor selection is achieved using two different deep reinforcement learning methods: 1) the cross-entropy method (CEM) and 2) the deep deterministic policy gradient (DDPG) method. The framework and algorithms for applying these control methods are presented. Experiments were performed on a Duffing oscillator as it is a classic nonlinear dynamical system with multiple attractors. Both methods achieve attractor selection under various control constraints. While these methods have nearly identical success rates, the DDPG method has the advantages a high learning rate, low performance variance, and offers a smooth control approach. This experiment demonstrates the applicability of reinforcement learning to constrained attractor selection problems.

Keywords Coexisting attractors · Attractor selection · Reinforcement learning · Machine learning · Nonlinear dynamical system

1 Introduction

Coexisting solutions or stable attractors are a hallmark of nonlinear systems and appear in highly disparate scientific applications [1, 2, 3, 4, 5, 6, 7, 8]. For these systems with multiple attractors, there often exists a preferable solution and one or more less preferable, or potentially catastrophic, solutions [9]. For example, many nonlinear energy harvesters have multiple attractors, each with different levels of power output, among which the largest one is typically desired [10, 11, 12]. Another example is the coexistence of period-1 and period-2 rhythms in cardiac dynamics. Controlling the trajectory of the cardiac rhythm to period-1 is desirable to avoid arrhythmia [13, 14]. Furthermore, coexisting solutions also appear in ecology and represent various degrees of ecosystem biodiversity [15], where a bio-manipulation scheme is needed to avoid certain detrimental environmental states [16].

These and other applications have motivated the development of several control methods to switch between attractors of nonlinear dynamical systems. Pulse control is one of the simplest methods; it applies a specific type of perturbation to direct a system's trajectory from one basin of attraction to another and waits until the trajectory settles down to the desired attractor [17, 18, 19]. Targeting algorithms, which were presented by Shinbrot et al. and modified by Macau et al., exploit the exponential sensitivity of basin boundaries in chaotic systems to small perturbations to direct the trajectory to a desired attractor in a short time [20, 21]. Lai developed an algorithm to steer most trajectories to a desired attractor using small feedback control, which builds a hierarchy of paths towards the desirable attractor and then stabilizes a trajectory around one of the paths [22]. Besides switching between naturally stable attractors, one can also stabilize the unstable periodic orbits and switch between these stabilized attractors. Since the OGY method was devised by Ott, Grebogi, and Yorke in 1990 [23], numerous works have built upon this original idea and explored relevant applications [24, 25, 26, 27, 28, 29].

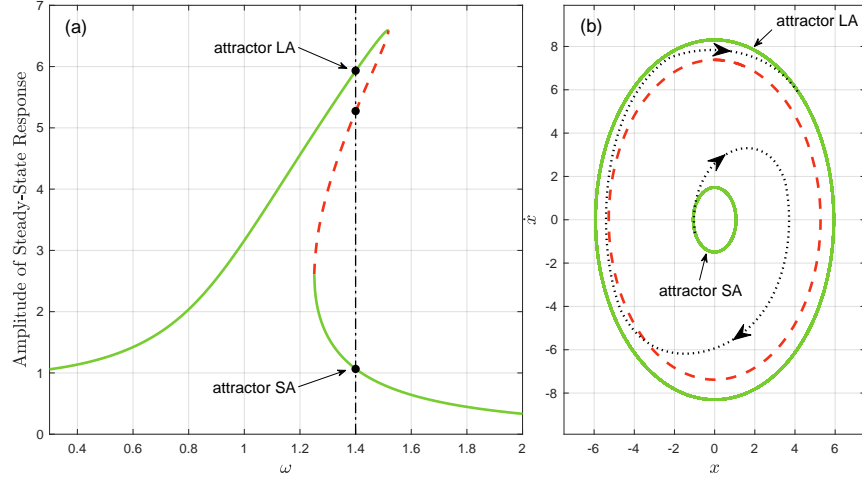


Figure 1: Coexisting attractors for the hardening Duffing oscillator: $\ddot{x} + 0.1\dot{x} + x + 0.04x^3 = \cos\omega t$. (a) Frequency responses. (b) Phase portrait of coexisting solutions when $\omega = 1.4$. Within a specific range of frequency, periodic solutions coexist in (a), including two stable solutions (green solid lines) and an unstable solution (red dashed line) in-between. The stable solutions correspond to an attractor with small amplitude (SA) and the other one with large amplitude (LA). The dotted line in (b) is a trajectory of switching attractor $SA \rightarrow LA$ using the control method introduced in this paper.

Although these methods can work for certain categories of problems, they are subject to at least one of the following restrictions: (1) they only work for chaotic systems; (2) they only work for autonomous systems; (3) they need existence of unstable fixed points; (4) they cannot apply constraints to control; or (5) they cannot apply control optimization. Especially for the last two limitations, the compatibility with constrained optimal control is difficult to realize for most methods mentioned yet plays an important role in designing a real-world controller. For example, the limitations on the instantaneous power/force and total energy/impulse of a controller need be considered in practice. Another practical consideration is the optimization of total time and energy spent on the control process. Switching attractors using as little time or energy as possible is oftentimes required, especially when attempting to escape detrimental responses or using a finite energy supply.

Fortunately, a technique that is compatible with a broader scope of nonlinear systems, reinforcement learning (RL), can be applied without the aforementioned restrictions [30]. By learning action-decisions while optimizing the long-term consequences of actions, RL can be viewed as an approach to optimal control of nonlinear systems [31]. Various control constraints can also be applied by carefully defining a reward function in RL [32]. Although several studies of attractor selection using RL were published decades ago [33, 34, 35], they dealt with only chaotic systems with unstable fixed points due to the limited choice of RL algorithms at the time. In recent years, a large number of advanced RL algorithms have been created to address complex control tasks. This paper will apply two of them, the cross-entropy method (CEM) and deep deterministic policy gradient (DDPG), to investigate the problem of attractor selection for a representative nonlinear dynamical system.

2 Reinforcement Learning (RL) Framework

In RL, an *agent* gains experience by making *observations*, taking *actions* and receiving *rewards* from an *environment*, and then learns a *policy* from past experience to achieve goals (usually maximized cumulative *reward*). As a representative system possessing coexisting solutions, the Duffing oscillator was chosen to demonstrate attractor selection via RL.

Environment. A harmonically forced Duffing oscillator, which can be described by the equation $\ddot{x} + \delta\dot{x} + \alpha x + \beta x^3 = \gamma \cos \omega t$, provides a familiar example for exploring the potential of RL for attractor selection. Fig. 1 shows an example of a hardening ($\alpha > 0, \beta > 0$) frequency response. For certain ranges of the parameters, the frequency response is a multiple-valued function of ω , which represents multiple coexisting steady-state oscillations at a given forcing frequency. With a long-run time evolution, the oscillation of the unstable solution cannot be maintained due to inevitable small perturbations. The system will always eventually settle into one of the stable steady-state responses of the system, which are therefore considered “attractors”. Our objective is to apply control to the Duffing oscillator to make it switch between the two attractors using constrained actuation.

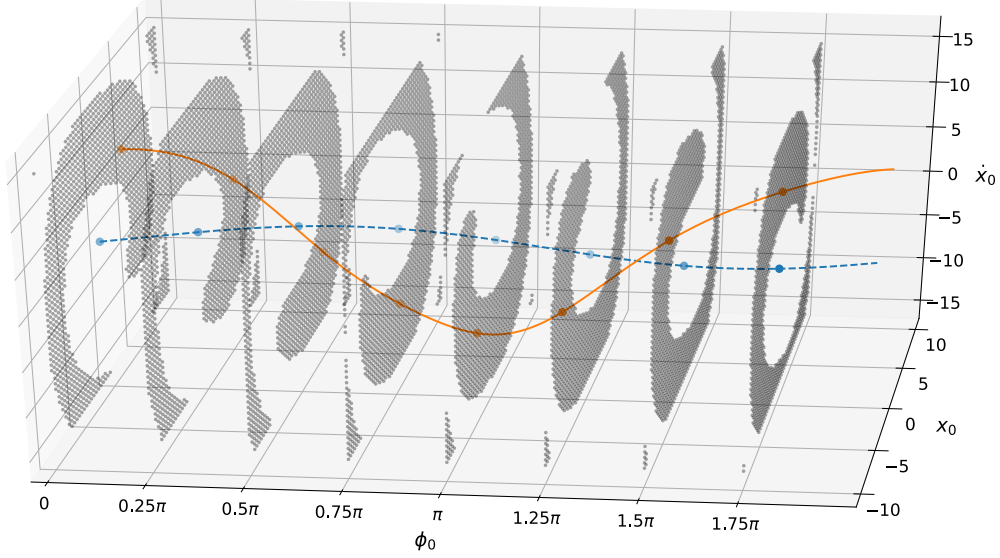


Figure 2: Basins of attraction (BoA) determined by the Duffing oscillator’s state variables, $[x, \dot{x}, \phi]$. Each point in the BoA represents an initial condition which drives the system to a certain attractor without control. The orange solid line and the shaded areas are the large-amplitude attractor and its corresponding BoA, respectively. The blue dashed line and the blank areas are the small-amplitude attractor and its corresponding BoA, respectively.

To provide actuation for attractor selection, an additional term $a(s)$, is introduced into the governing equation:

$$\ddot{x} + \delta\dot{x} + \alpha x + \beta x^3 = \gamma \cos(\omega t + \phi_0) + a(s). \quad (1)$$

where $a(s)$ is the actuation which depends on the system’s states s . For example, if the Duffing oscillator is a mass–spring–damper system, $a(s)$ represents a force.

Action. Aligned with the practical consideration that an actuation is commonly constrained, the action term can be written as $a(s) := F\pi_\theta(s)$, where F is the action bound which denotes the maximum absolute value of the actuation and $\pi_\theta(s)$ is the control policy. $\pi_\theta(s)$ is designed to be a function parameterized by θ , which has an input of the Duffing oscillator’s states s , and an output of a actuation scaling value between -1 and 1 . Our objective is achieved by finding qualified parameters θ that cause the desired attractor to be selected.

State & Observation. The Duffing oscillator is driven by a time-varying force $\gamma \cos \omega t$; thus, the state should consist of position x , velocity \dot{x} , and time t . Given that $\gamma \cos \omega t$ is a sinusoidal function with a phase periodically increasing from 0 to 2π , time can be replaced by phase for a simpler state expression. The system’s state can therefore be written as $s := [x, \dot{x}, \phi]$, where ϕ is equal to ωt modulo 2π . For the sake of simplicity, we have assumed no observation noise was introduced and the states were fully observable by the agent.

Reward. A well-trained policy should use a minimized control effort to reach the target attractor; thus the reward function, which is determined by state s_t and action a_t , should inform the cost of the action taken and whether the Duffing oscillator reaches the target attractor. The action cost is defined as the impulse given by the actuation, $a_t \Delta t$, where Δt is the time step size for control. The environment estimates whether the target attractor will be reached by evaluating the next state s_{t+1} . A constant reward of r_{end} is given only if the target attractor will be reached.

For estimating whether the target attractor will be reached, one could observe whether s_{t+1} is in the “basin of attraction” of the target attractor. Basins of attraction (BoA) are the sets of initial states leading to their corresponding attractors as time evolves (see Fig. 2). Once the target BoA is reached, the system will automatically settle into the desired stable trajectory without further actuation. Therefore, the reward function can be written as:

$$r(s_t, a_t) = -a_t \Delta t + \begin{cases} r_{\text{end}}, & \text{if } s_{t+1} \text{ reaches target BoA} \\ 0, & \text{otherwise} \end{cases} \quad (2)$$

BoA Classification. Knowing whether the system reaches the target BoA is non-trivial. For an instantaneous state $s_t = [x_t, \dot{x}_t, \phi_t]$, we could set $a(s) = 0$ in Eq. (1) and integrate it with the initial condition $[x_0, \dot{x}_0, \phi_0] = s_t$. Integrating for a sufficiently long time should give a steady-state response, whose amplitude can be evaluated to inform

on which attractor the system will settle down and whether s_t reaches the target BoA. However, this prediction is needed for each time step of the reinforcement learning process and the integration time should be sufficiently long to obtain steady-state responses; thus this approach results in expensive computational workload and a slow learning process. To obviate the expensive computational process, we realized a more efficient method was required to determine which final attractor corresponded to the system’s current state.

Since the number of attractors is finite, the attractor prediction problem can be considered a classification problem, which has an input of the system’s state and an output of the attractor class. Given that the boundary of basins is nonlinear as shown in Fig. 2, the classification method of support vector machines (SVM) with Gaussian kernel was selected for the Duffing oscillator. For other nonlinear dynamical systems, logistic regression is recommended for a linear boundary of basins and a neural network is recommended for a large number of attractors. The training data was created by sampling states uniformly on the domain of three state variables, and the attractor label for each state was determined by the method mentioned above: evaluating future responses with long-term integration of governing equation. Generally speaking, this method transfers the recurring cost of integration during the reinforcement learning process to a one-time cost before the learning process begins. Collecting and labeling the data for training the classifier can be time consuming, but once the classifier is well-trained, the time for predicting the final attractor can be negligibly small.

3 Algorithms

This section describes two RL algorithms for attractor selection, the cross-entropy method (CEM) and deep deterministic policy gradient (DDPG). These two methods were selected for their ability to operate over continuous action and state spaces [36]. This section will first explain a few important terms before describing the specifics of each algorithm.

Phase 1: the phase where the system is free of control, i.e., $a(s) = 0$. The system is given a random initial condition at the beginning of Phase 1, waits for dissipation of transient, and settles down on the initial attractor at the end of Phase 1.

Phase 2: the phase following Phase 1; the system is under control. Phase 2 starts with the system running in the initial attractor, and ends with either reaching the target BoA or exceeding time limit.

Trajectory: the times series of state-action pairs, $[s_t, a_t]$, in Phase 2. The data of trajectories are stored in a *Replay Buffer*.

The entire process for learning a control policy can be summarized as iterative episodes. In each episode, the system runs through Phase 1 and Phase 2 in turn and the control policy is improved using the data of trajectories stored in the replay buffer. CEM and DDPG are different methods for updating the control policy.

The cross-entropy method (CEM) was pioneered as a Monte Carlo method for importance sampling, estimating probabilities of rare events in stochastic networks [37, 38]. Learning a control policy for attractor selection using the CEM consists of repeating the following four steps: (1) generate N sample trajectories using the current control policy π_θ with exploration noise; (2) evaluate each of these N sampled trajectories with its cumulative reward R ; (3) select N' elite sample trajectories with the highest R , where $N' < N$; (4) refit π_θ to the elite samples by updating the policy’s parameters θ . The detailed attractor selection algorithm using CEM can be found in Tab. 1 in the supplemental material.

Deep Deterministic Policy Gradient (DDPG) is a RL algorithm based on the deterministic policy gradient that can operate over continuous action spaces [39]. One major difference between CEM and DDPG is the usage of the policy gradient, which can be considered the derivative of the cumulative reward with respect to the policy parameters, $\nabla_\theta \sum_t r(s_t, a_t)$. The CEM is a gradient-free algorithm while the DDPG computes the gradient for policy updating. Another difference lies in their approach to using stored data. The CEM improves the policy after collecting new trajectories of data, while the DDPG continuously improves the policy at each time step as it explores the environment [36]. The detailed attractor selection algorithm using CEM can be found in Tab. 2 in the supplemental material.

4 Experimental Results

To test the CEM and DDPG algorithms, constraints were constructed with varying levels of difficulty, i.e., different action bound F . Recall that the control term in Eq. (1) can be written as $a(s) = F\pi_\theta(s)$, which is bounded between $-F$ and F . It’s also worth noting that each policy only controls a one-way trip of attractor switching. For the example of a Duffing oscillator with two attractors, one control policy is needed for transitioning from the small-amplitude attractor to the large-amplitude one, and another control policy is needed for the reverse direction. Fig. 3 and Fig. 4 show the

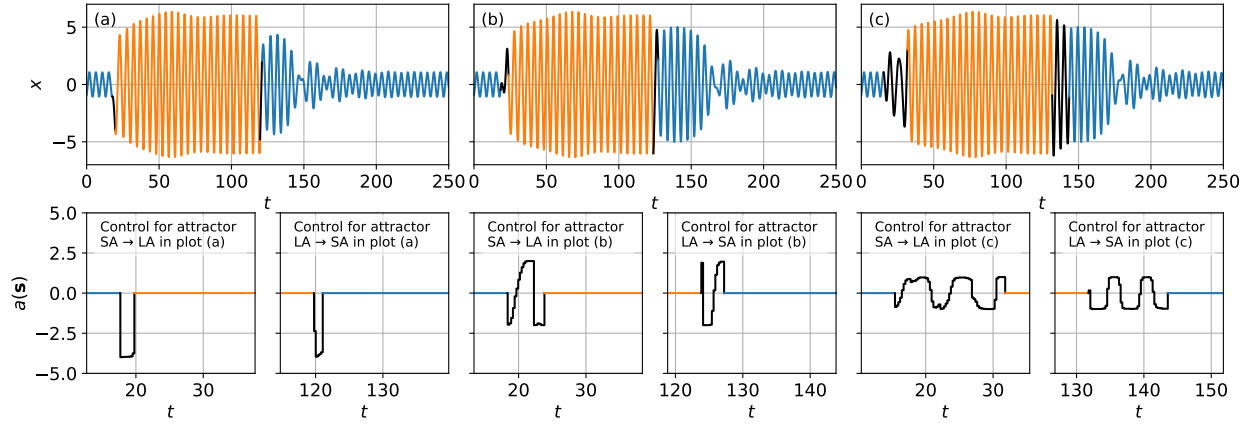


Figure 3: Attractor selection control policy learned by CEM with varying action bounds: (a) $F = 4$, (b) $F = 2$, (c) $F = 1$. Blue lines represent the Duffing oscillator running in the basin of attractor SA, which has a periodic solution with small amplitude. Orange lines represent the Duffing oscillator running in the basin of attractor LA, which has a periodic solution with large amplitude. Black lines represent the Duffing oscillator under control. Each plot of the system's responses in the first row corresponds to the two sub-plots of controlling processes in the second row: attractor $SA \rightarrow LA$ and attractor $LA \rightarrow SA$.

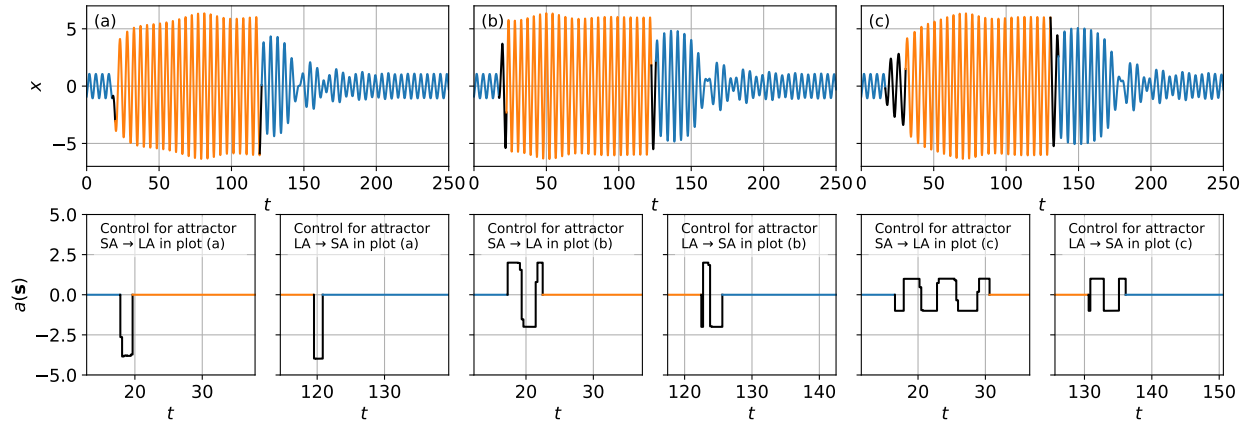


Figure 4: Attractor selection control policy learned by DDPG with varying action bounds: (a) $F = 4$, (b) $F = 2$, (c) $F = 1$. Blue lines represent the Duffing oscillator running in the basin of attractor SA, which has a periodic solution with small amplitude. Orange lines represent the Duffing oscillator running in the basin of attractor LA, which has a periodic solution with large amplitude. Black lines represent the Duffing oscillator under control. Each plot of the system's responses in the first row corresponds to the two sub-plots of controlling processes in the second row: attractor $SA \rightarrow LA$ and attractor $LA \rightarrow SA$.

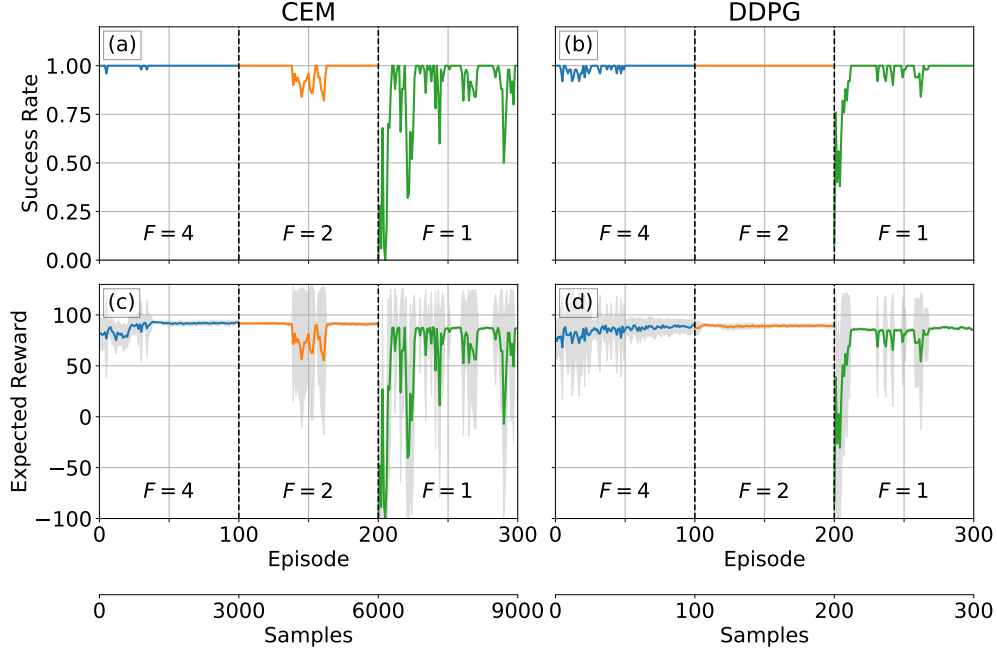


Figure 5: The control policy performance curve for the success rate of reaching target attractor using (a) CEM and (b) DDPG, and the expected accumulated reward of a control process using (c) CEM and (d) DDPG. The varying action bound of 4, 2, and 1 are represented by the blue, orange, and green lines respectively. The gray areas in plot (c) and (d) represent standard deviation of the accumulated rewards.

time series of attractor selection using the control policy learned by the CEM and DDPG algorithms, respectively. For simplicity, the attractor with a small amplitude of steady-state response is named “SA” while that with a large amplitude is named “LA”. More experiment details (such as environment parameters, neural network structures, etc.) can be found in the supplemental material.

For all six test cases in Fig. 3 and Fig. 4, the Duffing oscillator starts near the SA solution, then switches from SA to LA, and finally switches backwards from LA to SA. Compared with the short time length for control (region of black lines), the attractor selection spends more time waiting for dissipation of the transient process, where the system is automatically approaching the target attractor under no control. This observation shows a smart and efficient strategy the control policy has learned: instead of driving the system precisely to the state set of the target attractor, it just drives the system to the attractor’s basin, where the system might be far away from the target attractor initially but will reach it without further control effort as time evolves.

One can also observe that a smaller action bound results in a longer time length of control for both CEM and DDPG algorithms. It can be qualitatively explained by the energy threshold for jumping from one attractor to another. The energy provided by the actuation should be accumulated beyond the energy threshold to push the system away from one attractor. A smaller action bound therefore leads to longer time for the energy accumulation. Another observation is that the system quickly approaches near LA when starting from SA, while it takes more time to approach near SA when starting from LA. This can be explained using the unstable solution of Duffing equation which is represented as the red dashed circle in Fig. 1 (b). This circle can be considered the boundary between the basins of two attractors, across which the system jumps from one attractor to another. This boundary is close to LA, which means that the system will be near LA immediately after going across the boundary from SA. In contrast, SA is far from the boundary; therefore, a longer time is needed to reach near SA after going across the boundary from LA.

Although the CEM and DDPG algorithms both achieve attractor selection with various action bounds, DDPG has advantages of providing smooth actuations. From the comparison of the actuation $F\pi_\theta(s)$ between Fig. 3 and Fig. 4, the actuation from CEM shows more jagged motion than that from DDPG especially for the small action bound. More advantages of DDPG over CEM can be observed in Fig. 5, which compares the trend of their policies’ success rate and expected reward during learning process. In each learning episode, 100 samples with random initial states were used to evaluate the control policy’s success rate of reaching target attractor, and the mean and standard deviation of the samples’ accumulated reward. For faster convergence, the policy trained for a tighter action bound was initialized with

the parameters of a well-trained policy for a more generous action bound. In other words, instead of learning from zero, a policy learns to solve a hard problem from the experience of solving an easy one. The “untrained” policy for the action bound of 2 was initialized with the parameters of the “trained” policy for the action bound of 4, and so on. Therefore in Fig. 5, the action bound decreases as the learning episode increases.

The success rates and expected rewards are equally high for both CEM and DDPG at the end of the learning episode for each action bound (episode = 100, 200, 300), but DDPG converges faster, especially for the action bound of 1. This advantage of DDPG can be observed from the performance curve which evolves with “episode” in Fig. 5, but DDPG is even better than this considering that it spends much less time on each episode than CEM. As shown in the detailed algorithms in the supplemental material, CEM (see Table 1) needs N samples of trajectories for updating the policy in each episode, while DDPG (see Table 2) collects only the sample of a single trajectory. The real learning speed can therefore be reflected by the total “samples” generated instead of “episode”. Fig. 5 shows the DDPG’s advantage of learning speed and data efficiency by providing an additional horizontal axis for the number of samples, where CEM generates 30 samples per episode while DDPG generates only 1 sample per episode. Parallel computing can be used for helping CEM narrow the gap, but generally DDPG has a natural advantage of learning speed. Furthermore, after the CEM learned an optimal policy, it often degenerated to a sub-optimal policy, which can be observed from the small perturbation around episode 150 and the significant oscillation throughout episode 200–300 in Fig. 5 (b,d). In contrast, DDPG shows a lower variance of the policy performance after an optimal policy has been learned, which can be observed from the flat line in episode 100–200 and the comparatively small perturbation in episode 200–300.

5 Conclusion

This work applies advanced reinforcement learning (RL) methods into the control problem of attractor selection, resulting in algorithms that switch between coexisting attractors of a nonlinear dynamical system using constrained actuation. A control framework was presented combining attractor selection and general RL methods. Two specific algorithms were designed based on cross-entropy method (CEM) and deep deterministic policy gradient (DDPG).

The Duffing oscillator, which is a classic nonlinear dynamical system with multiple coexisting attractors, was selected to demonstrate the control design and show the performance of the control policy learned by CEM and DDPG. Both methods achieved attractor selection under various constraints on actuation. They had equally high success rates, but DDPG had advantages of smooth control, high learning speed, and low performance variance.

The RL-based attractor selection is model-free and thus needs no prior knowledge on the system model. This provides broad applicability since a precise mathematical model for many real-world systems are often unavailable due to their highly nonlinear features or high noise level. A wider practicability results from the easy customization of control constraints. Apart from constraining the maximum actuation in the Duffing oscillator example, the system’s position can be constrained in case of working in a limited space, the system’s velocity can be constrained if there exists a hardware requirement of speed range, and the constraints themselves can even be time-varying. Various constraints can be realized by carefully designing the action term and reward function.

A few limitations to our approach remain. Although the system’s model is unnecessary, the prior knowledge of the coexisting attractors and a method of estimating whether a state belongs to the target attractor’s basin are required. In addition, as with most control methods based on model-free RL, our method requires a large number of training samples to find a decent control policy, especially for CEM. A large amount of simulations or experiments could be costly and time-consuming.

References

- [1] John Michael Tutill Thompson and H Bruce Stewart. *Nonlinear dynamics and chaos*. John Wiley & Sons, 2002.
- [2] E. Brun, B. Derighetti, D. Meier, R. Holzner, and M. Ravani. Observation of order and chaos in a nuclear spin–flip laser. *J. Opt. Soc. Am. B*, 2(1):156–167, Jan 1985.
- [3] J Maurer and A Libchaber. Effect of the prandtl number on the onset of turbulence in liquid 4he. *Journal de Physique lettres*, 41(21):515–518, 1980.
- [4] Robert M May. Thresholds and breakpoints in ecosystems with a multiplicity of stable states. *Nature*, 269(5628):471, 1977.
- [5] JL Hudson and JC Mankin. Chaos in the belousov–zhabotinskii reaction. *The Journal of Chemical Physics*, 74(11):6171–6177, 1981.

- [6] Xue-She Wang, Michael J. Mazzoleni, and Brian P. Mann. Dynamics of unforced and vertically forced rocking elliptical and semi-elliptical disks. *Journal of Sound and Vibration*, 417:341 – 358, 2018.
- [7] Xue-She Wang and Brian P. Mann. Nonlinear dynamics of a non-contact translational-to-rotational magnetic transmission. *Journal of Sound and Vibration*, 459:114861, 2019.
- [8] Xue-She Wang and Brian P. Mann. Dynamics of a magnetically excited rotational system. In Gaetan Kerschen, M. R. W. Brake, and Ludovic Renson, editors, *Nonlinear Structures and Systems, Volume 1*, pages 99–102, Cham, 2020. Springer International Publishing.
- [9] Alexander N. Pisarchik and Ulrike Feudel. Control of multistability. *Physics Reports*, 540(4):167 – 218, 2014. Control of multistability.
- [10] B.P. Mann and N.D. Sims. Energy harvesting from the nonlinear oscillations of magnetic levitation. *Journal of Sound and Vibration*, 319(1):515 – 530, 2009.
- [11] Samuel C. Stanton, Clark C. McGehee, and Brian P. Mann. Nonlinear dynamics for broadband energy harvesting: Investigation of a bistable piezoelectric inertial generator. *Physica D: Nonlinear Phenomena*, 239(10):640 – 653, 2010.
- [12] Samuel C Stanton, Clark C McGehee, and Brian P Mann. Reversible hysteresis for broadband magnetopiezoelastic energy harvesting. *Applied Physics Letters*, 95(17):174103, 2009.
- [13] Richard P Kline and B Mitchell Baker. A dynamical systems approach to membrane phenomena underlying cardiac arrhythmias. *International Journal of Bifurcation and Chaos*, 5(01):75–88, 1995.
- [14] Ali R Yehia, Dominique Jeandupeux, Francisco Alonso, and Michael R Guevara. Hysteresis and bistability in the direct transition from 1: 1 to 2: 1 rhythm in periodically driven single ventricular cells. *Chaos: An Interdisciplinary Journal of Nonlinear Science*, 9(4):916–931, 1999.
- [15] Marten Scheffer, Steve Carpenter, Jonathan A Foley, Carl Folke, and Brian Walker. Catastrophic shifts in ecosystems. *Nature*, 413(6856):591, 2001.
- [16] Egbert H Van Nes and Marten Scheffer. Slow recovery from perturbations as a generic indicator of a nearby catastrophic shift. *The American Naturalist*, 169(6):738–747, 2007.
- [17] Kuniyiko Kaneko. Chaotic but regular posi-nega switch among coded attractors by cluster-size variation. *Physical Review Letters*, 63(3):219, 1989.
- [18] Kuniyiko Kaneko. Clustering, coding, switching, hierarchical ordering, and control in a network of chaotic elements. *Physica D: Nonlinear Phenomena*, 41(2):137 – 172, 1990.
- [19] AM Samson, SI Turovets, VN Chizhevsky, and VV Churakov. Nonlinear dynamics of a loss-switched co2 laser. *Sov. Phys. JETP*, 74(4):628–639, 1992.
- [20] Troy Shinbrot, Edward Ott, Celso Grebogi, and James A Yorke. Using chaos to direct trajectories to targets. *Physical Review Letters*, 65(26):3215, 1990.
- [21] Elbert E. N. Macau and Celso Grebogi. Driving trajectories in complex systems. *Phys. Rev. E*, 59:4062–4070, Apr 1999.
- [22] Ying-Cheng Lai. Driving trajectories to a desirable attractor by using small control. *Physics Letters A*, 221(6):375–383, 1996.
- [23] Edward Ott and Mark Spano. Controlling chaos. In *AIP Conference Proceedings*, volume 375, pages 92–103. AIP, 1996.
- [24] Fernando Casas and Celso Grebogi. Control of chaotic impacts. *International Journal of Bifurcation and Chaos*, 7(04):951–955, 1997.
- [25] Elbert EN Macau and Celso Grebogi. Control of chaos and its relevancy to spacecraft steering. *Philosophical Transactions of the Royal Society A: Mathematical, Physical and Engineering Sciences*, 364(1846):2463–2481, 2006.
- [26] Troy Shinbrot, Celso Grebogi, James A Yorke, and Edward Ott. Using small perturbations to control chaos. *nature*, 363(6428):411, 1993.
- [27] Kazuyuki Yagasaki and Tomotsugu Uozumi. A new approach for controlling chaotic dynamical systems. *Physics Letters A*, 238(6):349–357, 1998.
- [28] Bogdan I Epureanu and Earl H Dowell. On the optimality of the ott-grebogi-yorke control scheme. *Physica D: Nonlinear Phenomena*, 116(1-2):1–7, 1998.

- [29] DL Hill. On the control of chaotic dynamical systems using nonlinear approximations. *International Journal of Bifurcation and Chaos*, 11(01):207–213, 2001.
- [30] James D. Turner, Levi H. Manning, and Brian P. Mann. Reinforcement learning for active damping of harmonically excited pendulum with highly nonlinear actuator. In Gaetan Kerschen, M. R. W. Brake, and Ludovic Renson, editors, *Nonlinear Structures and Systems, Volume 1*, pages 119–123, Cham, 2020. Springer International Publishing.
- [31] Chung Chen and Chi-Cheng Jou. A reinforcement learning control scheme for nonlinear systems with multiple actions. In *Soft Computing in Intelligent Systems and Information Processing. Proceedings of the 1996 Asian Fuzzy Systems Symposium*, pages 43–48, Dec 1996.
- [32] R. S. Sutton, A. G. Barto, and R. J. Williams. Reinforcement learning is direct adaptive optimal control. *IEEE Control Systems Magazine*, 12(2):19–22, April 1992.
- [33] R Der and N Herrmann. Q-learning chaos controller. In *Proceedings of 1994 IEEE International Conference on Neural Networks (ICNN'94)*, volume 4, pages 2472–2475. IEEE, 1994.
- [34] Sabino Gadaleta and Gerhard Dangelmayr. Optimal chaos control through reinforcement learning. *Chaos: An Interdisciplinary Journal of Nonlinear Science*, 9(3):775–788, 1999.
- [35] Sabino Gadaleta and Gerhard Dangelmayr. Learning to control a complex multistable system. *Physical Review E*, 63(3):036217, 2001.
- [36] Yan Duan, Xi Chen, Rein Houthooft, John Schulman, and Pieter Abbeel. Benchmarking deep reinforcement learning for continuous control. In *International Conference on Machine Learning*, pages 1329–1338, 2016.
- [37] Reuven Y. Rubinstein. Optimization of computer simulation models with rare events. *European Journal of Operational Research*, 99(1):89 – 112, 1997.
- [38] Reuven Rubinstein. The cross-entropy method for combinatorial and continuous optimization. *Methodology And Computing In Applied Probability*, 1(2):127–190, Sep 1999.
- [39] Timothy P Lillicrap, Jonathan J Hunt, Alexander Pritzel, Nicolas Heess, Tom Erez, Yuval Tassa, David Silver, and Daan Wierstra. Continuous control with deep reinforcement learning. *arXiv preprint arXiv:1509.02971*, 2015.
- [40] Xavier Glorot, Antoine Bordes, and Yoshua Bengio. Deep sparse rectifier neural networks. In *Proceedings of the fourteenth international conference on artificial intelligence and statistics*, pages 315–323, 2011.
- [41] Diederik P Kingma and Jimmy Ba. Adam: A method for stochastic optimization. *arXiv preprint arXiv:1412.6980*, 2014.

Supplemental Information: Constrained Attractor Selection Using Deep Reinforcement Learning

This section presents experiment details in the paper, which covers the environment configuration (i.e. the parameters of Duffing oscillator), detailed algorithms for attractor selection using CEM and DDPG, and structures of neural networks in the two algorithms.

The governing equation for the Duffing oscillator is given by:

$$\ddot{x} + \delta \dot{x} + \alpha x + \beta x^3 = \gamma \cos(\omega t + \phi_0) + a(\mathbf{s}). \quad (3)$$

where $\delta = 0.1$, $\alpha = 1$, $\beta = 0.04$, $\gamma = 1$ and $\omega = 1.4$. The Duffing equation is integrated using `scipy.integrate.odeint()` in Python with a time step length of 0.01. The time step length for control is 0.25, and reaching the target BoA will add a reward $r_{\text{end}} = 100$. Therefore, the reward function can be written as:

$$r(\mathbf{s}_t, a_t) = \begin{cases} 100 - 0.25a_t, & \text{if } \mathbf{s}_{t+1} \text{ reaches target BoA} \\ -0.25a_t, & \text{otherwise} \end{cases} \quad (4)$$

The SVM classifier with radial basis function (RBF) kernel was trained by using $50^3 = 125000$ initial conditions, where 50 evenly distributed values were sampled for each state variables, $x \in [-10, 10]$, $\dot{x} \in [-15, 15]$ and $\phi \in [0, 2\pi]$.

The detailed attractor selection algorithm using CEM can be found in Tab. 1. In line 11, the time of Phase 1 is perturbed by adding a random value between 0 and $2\pi/\omega$ (a forcing period). This noise provides diversity of the system’s states at the beginning of Phase 2, which enhances generality and helps prevent over-fitting of the control policy network $\pi_\theta(\mathbf{s})$. The policy network $\pi_\theta(\mathbf{s})$ has two hidden layers, each of which has 64 units and an activation function of ReLU [40]. The final output layer is a tanh layer to bound the actions. Adam optimizer [41] with a learning rate of 10^{-3} and a minibatch size of 128 were used for learning the neural network parameters. For the system’s settling down in Phase 1 we used $T_1 = 15$, and for constraining the time length of control we used $T_2 = 20$. In each training episode, state-action pairs from 30 trajectory samples was stored in the replay buffer ($N = 30$), and those with top 80% of reward were selected for training the network ($p = 0.8$).

The detailed attractor selection algorithm using DDPG can be found in Tab. 2. Apart from the “actor” network $\pi_\theta(\mathbf{s})$ which is same as the policy network in the CEM, the DDPG introduces an additional “critic” network $Q_\psi(\mathbf{s}, a)$. This Q network is designed to be a neural network parameterized by ψ , which has two inputs of the system’s state and corresponding action, and an output of a scalar (has a name of “Q-value” in reinforcement learning). Same as the algorithm using CEM, the state diversity is promoted by introducing noise to the time of Phase 1 in line 9. Both of the actor network $\pi_\theta(\mathbf{s})$ and the critic network $Q_\psi(\mathbf{s}, a)$ have two hidden layers, each of which has 128 units and an activation function of ReLU [40]. For the actor network, the final output layer is a tanh layer to bound the actions. For the critic network, the input layer consists of only the state \mathbf{s} , while the action a is included in the 2nd hidden layer. Adam optimizer [41] was used to learn the neural network parameters with a learning rate of 10^{-4} and 10^{-3} for the actor and critic respectively. For the update of critic network we used a discount factor of $\gamma = 0.9$. For the soft update of the target network $\pi_{\theta'}(\mathbf{s})$ and $Q_{\psi'}(\mathbf{s}, a)$, we used $\tau = 0.1$. For the system’s settling down in Phase 1 we used $T_1 = 15$, and for constraining the time length of control we used $T_2 = 20$. The replay buffer has a size of 10^6 . In each episode, the minibatch of transitions sampled from the replay buffer has a size of $N = 64$.

Table 1: Algorithm: Cross-Entropy Method (CEM) for Attractor Selection

1	Randomly initialize policy network $\pi_\theta(\mathbf{s})$ with weight θ	
2	Set the initial condition of Duffing equation $\mathbf{s}_0 = [x_0, \dot{x}_0, \phi_0]$	
3	Set time of Phase 1 and Phase 2, T_1 and T_2	
4	Set best sample proportion, $p \in [0, 1]$	
5	for episode = 1 : M do	
6	Initialize an empty replay buffer B	
7	for sample = 1 : N do	
8	Initialize an empty buffer \tilde{B}	
9	Initialize a random process \mathcal{N} for action exploration	
10	Initialize trajectory reward, $R = 0$	
11	Add noise to time of Phase 1, $T_1' = T_1 + \text{random}(0, 2\pi/\omega)$	
12	Integrate Eq. (3) for $t \in [0, T_1']$ with $a(\mathbf{s}) = 0$	Phase 1
13	for $t = T_1' : T_1' + T_2$ do	Phase 2
14	Observe current state, $\mathbf{s}_t = [x_t, \dot{x}_t, \phi_t]$	
15	Evaluate action $a_t(\mathbf{s}_t) = F\pi_\theta(\mathbf{s}_t) + \mathcal{N}_t$, according to the current policy and exploration noise	
16	Step into the next state \mathbf{s}_{t+1} , by integrating Eq. (3) for Δt	
17	Update trajectory reward $R \leftarrow R + r(\mathbf{s}_t, a_t)$, according to Eq. (4)	
18	Store state-action pair $[\mathbf{s}_t, a_t]$ in \tilde{B}	
19	Evaluate the basin of attractor with \mathbf{s}_{t+1}	
20	if the target attractor's basin is reached:	
21	Label each state-action pair $[\mathbf{s}_t, a_t]$ in \tilde{B} with trajectory reward R , and append them to B	
22	break	
23	end for	
24	end for	
25	Choose the a minibatch of the elite p proportion of (\mathbf{s}, a) in B , with the largest reward R	
26	Update policy $\pi_\theta(\mathbf{s})$ by minimizing the loss, $L = \frac{1}{\text{Minibatch Size}} \sum_i (F\pi_\theta(\mathbf{s}_i) - a_i)^2$	
27	end for	

Table 2: Algorithm: Deep Deterministic Policy Gradient (DDPG) for Attractor Selection

1	Randomly initialize actor network $\pi_\theta(\mathbf{s})$ and critic network $Q_\psi(\mathbf{s}, a)$ with weights θ and ψ	
2	Initialize target network $\pi'_{\theta'}(\mathbf{s})$ and $Q'_{\psi'}(\mathbf{s}, a)$ with weights $\theta' \leftarrow \theta, \psi' \leftarrow \psi$	
3	Set the initial condition of Duffing equation $\mathbf{s}_0 = [x_0, \dot{x}_0, \phi_0]$	
4	Set discount factor γ , and soft update factor τ	
5	Set time of Phase 1 and Phase 2, T_1 and T_2	
6	Initialize replay buffer B	
7	for episode = 1 : M do	
8	Initialize a random process \mathcal{N} for action exploration	
9	Add noise to time of Phase 1, $T_1' = T_1 + \text{random}(0, 2\pi/\omega)$	
10	Integrate Eq. (3) for $t \in [0, T_1']$ with $a(\mathbf{s}) = 0$	Phase 1
11	for $t = T_1' : T_1' + T_2$ do	Phase 2
12	Observe current state, $\mathbf{s}_t = [x_t, \dot{x}_t, \phi_t]$	
13	Evaluate action $a_t(\mathbf{s}_t) = F\pi_\theta(\mathbf{s}_t) + \mathcal{N}_t$, according to the current policy and exploration noise	
14	Step into the next state \mathbf{s}_{t+1} , by integrating Eq. (3) for Δt	
15	Evaluate reward $r_t(\mathbf{s}_t, a_t)$, according to Eq. (4)	
16	Store transition $[\mathbf{s}_t, a_t, r_t, \mathbf{s}_{t+1}]$ in B	
17	Sample a random minibatch of N transitions $[\mathbf{s}_i, a_i, r_i, \mathbf{s}_{i+1}]$ from B	
18	Set $y_i = r_i + \gamma Q'_{\psi'}(\mathbf{s}_{i+1}, F\pi'_{\theta'}(\mathbf{s}_{i+1}))$	
19	Update critic network by minimizing the loss:	
	$L = \frac{1}{N} \sum_i (y_i - Q_\psi(\mathbf{s}_i, a_i))^2$	
20	Update the actor network using the sampled policy gradient:	
	$\nabla_\theta J = \frac{1}{N} \sum_i \nabla_a Q_\psi(\mathbf{s}, a) _{\mathbf{s}=\mathbf{s}_i, a=F\pi_\theta(\mathbf{s}_i)} \nabla_\theta \pi_\theta(\mathbf{s}) _{\mathbf{s}=\mathbf{s}_i}$	
21	Update the target networks:	
	$\psi' \leftarrow \tau\psi + (1-\tau)\psi', \theta' \leftarrow \tau\theta + (1-\tau)\theta'$	
22	if the target attractor's basin is reached in \mathbf{s}_{t+1} : break	
23	end for	
